

## **Recent Progress in Noise Thermometry at 505 K and 693 K Using Quantized Voltage Noise Ratio Spectra**

**W. L. Tew<sup>1</sup>, S. P. Benz<sup>2</sup>, P. D. Dresselhaus<sup>2</sup>, K. Coakley<sup>2</sup>, H. Rogalla<sup>3</sup>, D. R. White<sup>4</sup>, and J. R. Labenski<sup>5</sup>**

<sup>1</sup> NIST, Gaithersburg, MD USA

<sup>2</sup> NIST, Boulder CO USA

<sup>3</sup> University of Twente, Enschede, The Netherlands

<sup>4</sup> Measurement Standards Laboratory, Lower Hutt, New Zealand

<sup>5</sup> BAE Systems, Arlington, VA USA

E-mail (corresponding author): wtew@nist.gov

**Abstract**

We report on technical advances and new results in noise thermometry at temperatures near the tin freezing point and the zinc freezing point using a Quantized Voltage Noise Source (QVNS). The temperatures are derived in a series of separate measurements comparing the spectral power density of QVNS synthesized noise with that of Johnson noise from a known resistance at both 505 K and 693 K. Reference noise is digitally synthesized so that the average power spectra of the QVNS match those of the thermal noise, resulting in power ratio spectra which are close to unity in the low-frequency limit. Three-parameter models are used to account for differences in impedance-related time constants. Direct comparison of noise temperatures to ITS-90 is achieved in a comparison furnace with standard platinum resistance thermometers. We report on the observed noise temperatures determined by operating the noise thermometer in both absolute and relative modes, and related statistics together with estimated uncertainties. The relative noise thermometry results are combined with results from other thermodynamic determinations at temperatures near the tin freezing point to calculate a value of  $T - T_{90} = +4 \pm 18$  mK for temperatures near the zinc freezing point. These new results achieve a lower uncertainty than that of our earlier efforts and we compare the present value of  $T - T_{90}$  to other published determinations from noise thermometry and other methods.

**Keywords:** ITS-90; Johnson Noise Thermometry; Synthesized Noise Temperature;

## 1 Introduction

Recent technological improvements have enabled advances in Johnson Noise Thermometry (JNT) using Quantized Voltage Noise Sources [1]. These advances have been applied to our continuing efforts to determine thermodynamic temperatures  $T$  versus the International Temperature Scale of 1990 (ITS-90),  $T_{90}$  in the range 505 K to 693 K. In this paper we report on our most recent spectral noise-ratio data for these temperatures and compare the results to those obtained in our previous noise thermometry work [2][3].

The power spectral density of voltage fluctuations,  $S_R$ , in a metal conductor of resistance  $R$  at temperature  $T$  is given by the Nyquist approximation,

$$S_R = 4k_B TR, \quad (1)$$

where  $k_B$  is Boltzmann's constant. This noise is random, Gaussian, and remains white (frequency independent) out to frequencies  $\sim f_{\text{corr}} = 1/2\pi\tau_{\text{corr}}$  where  $\tau_{\text{corr}}$  is the time scale below which electron motions become correlated. Typically,  $\tau_{\text{corr}} = 3 \times 10^{-16}$  s due to collisions in resistive alloys, but quantum effects may occur on longer time scales such that  $\tau_{\text{corr}} \approx h/kT = 10^{-13}$  s at 505 K. Hence, even in the later case we would still expect Equation 1 to remain valid out to frequencies below  $f_{\text{corr}} \approx 1.7$  THz. In practice, however, such high cutoffs are never directly observable due to the limiting frequency response associated with other non-intrinsic time constants that are many orders of magnitude larger and governed by the unavoidable parasitic impedances of real macroscopic circuits and cables. In any case, Eq. 1 would still be expected to remain valid at 1 MHz and 500 K to better than  $1 \mu\text{K} \cdot \text{K}^{-1}$ .

Digitally synthesized noise waveforms can now be created via pulse-biased Josephson junction arrays forming a Quantized Voltage Noise Source (QVNS) [4]. The power spectral density  $S_Q$  of a QVNS array of  $N_J$  junctions operating at a sampling frequency  $f_s$  and a repetition rate  $f_1$  is given by

$$S_Q = \frac{D^2 N_J^2 f_s^2}{K_{J-90}^2 f_1}, \quad (2)$$

where  $K_J$  is the Josephson constant and  $D$  is a dimensionless parameter calculated from the digital synthesis.[5] This noise is non-random (i.e., deterministic) [6], approximately

Gaussian in the fluctuating (i.e. time-dependent) voltage amplitudes, and constructed to be of a constant average spectral density out to some maximum frequency  $f_{\max}$ .

If the ratio  $S_R/S_Q$  can be accurately measured, then it is possible to determine an absolute noise temperature  $T$  given by,

$$T = \frac{\langle S_R \rangle}{\langle S_Q \rangle} \frac{f_1 K_{J-90}^2}{4k_B R D^2 f_s^2 N_J^2} \quad (3)$$

This is the basis for JNT using a QVNS in the absolute mode [7].

In absolute mode, the noise signals are subject to differential filtering whenever the line and source impedances for the two sources are unmatched.[8] Imperfect impedance matching necessitates applying a frequency dependent correction where the factor  $\langle S_R \rangle / \langle S_Q \rangle$  in Eq. 3 is taken in the low frequency limit. In the lumped-impedance-parameter approximation, it is straightforward to show that the frequency correction will have the form,

$$\frac{\langle S_R \rangle}{\langle S_Q \rangle} \cong \frac{\langle S_R \rangle}{\langle S_Q \rangle} \Big|_0 \sum_{j=1} \left[ 1 + (\tau_{Qj}^j - \tau_{Rj}^j) \omega^j \right] \quad (4)$$

Where the  $\tau_Q$  and  $\tau_R$  are effective time constants associated with source, line, and input impedances for each of the two input networks. The R and Q input networks are primarily composed of: source/series resistances  $R(T)$ ,  $R_Q$ ; series inductances  $L_R$ ,  $L_Q$ ; and shunt capacitances  $C_R$ ,  $C_Q$ .[9] Ratio spectra are predominately quadratic below 1 MHz and the  $\tau_{Q2}$  and  $\tau_{R2}$  constants are dominated by  $RC$  and  $LC$  couplings. There are also small 4<sup>th</sup>-degree frequency terms where the  $\tau_{Q4}$  and  $\tau_{R4}$  constants are dominated by  $LC$  couplings.[10] The corresponding source impedances, however, do not couple in identical ways in the two networks, as the QVNS source decouples the two halves of that input network which halves the effective shunt capacitance compared to the analogous terms in the R network.[8] In practice, this correction is accomplished by statistical fitting of a simple polynomial model in frequency to the data, such as  $\langle S_R \rangle / \langle S_Q \rangle = a_0 + a_1 f + a_2 f^2 + a_3 f^3 + a_4 f^4$ , where the odd terms can often be ignored when dielectric losses are small.[9]

If noise power measurements are performed at two different temperatures,  $T_1$  and  $T_2$ , the ratio of the power spectra can be used to determine the temperature  $T_2$  in terms of  $T_1$ , which may be any convenient reference temperature. In this relative mode,  $T_2$  is given by,

$$T_2 = \frac{\langle S_{R,T2} \rangle \langle S_{Q1} \rangle}{\langle S_{Q2} \rangle \langle S_{R,T1} \rangle} \frac{D_1^2 R(T_1)}{D_2^2 R(T_2)} T_1 \quad (5)$$

The ratio  $T_2/T_1$ , while insensitive to many systematic errors that affect the absolute measurements, is subject to frequency response effects due to the time constants  $\tau_{R,j}(T)$  which are normally temperature dependent [11] and sometimes time dependent. By extension of the same parameterization of time constants of Eq. 4, we then have,

$$\frac{\langle S_{RT2} \rangle \langle S_{Q1} \rangle}{\langle S_{Q2} \rangle \langle S_{RT1} \rangle} \cong \frac{\langle S_{RT2} \rangle}{\langle S_{Q2} \rangle} \bigg|_0 \frac{\langle S_{Q1} \rangle}{\langle S_{RT1} \rangle} \bigg|_0 \sum_{j=1} \left[ 1 + (\tau_{R,j}^j(T_1) - \tau_{R,j}^j(T_2)) \omega^j \right] \quad (6)$$

All terms involving  $\tau_{Q,j}$  are cancelled in the relative mode, provided that all QVNS source input network impedances are stationary. The same approach to the parameterization of the correction model also applies in the relative mode case but the correction coefficients  $a_j$  ( $j > 0$ ) are usually much smaller than in the absolute case.

## 2 Experimental Systems

NIST maintains two operational JNT systems utilizing QVNS references. The first JNT system is located on the NIST Boulder CO campus and is optimized for operation at 273.16 K in the absolute mode with a fixed 100.0  $\Omega$  source resistance.[1][5] The second system is located on the NIST Gaithersburg MD campus and operates primarily in the relative mode in the range 505 K to 930 K with variable source impedances.[3] While the majority of our recent publications have described results obtained in the Boulder JNT system, this paper describes results obtained in the Gaithersburg system. Much of the electronics and QVNS-specific hardware in the two systems are similar but certain differences do exist and these will be noted where they affect specific measurement issues.

The experimental set up as shown in Figure 1 consists of: a QVNS system; a high-temperature-resistance probe; a digital-noise-voltage correlator; and a vacuum-comparison furnace system. All of the systems are housed in a electromagnetically-shielded facility on the Gaithersburg campus. Similar systems were in place at the Gaithersburg facility for our earlier

measurement as reported in 2008 [3], but several important changes and improvements have taken place since that work was completed.

## 2.1 QVNS

The QVNS used in the Gaithersburg JNT system is based on the same basic Josephson-junction technology as used in Boulder JNT systems. [12] The specific system described here is based on a dual array of 10 junctions each with critical currents of  $I_c(4.2\text{ K}) \cong 4.8\text{ mA}$  and four (two for each channel)  $R_Q = 97\ \Omega$  on-chip series resistor terminations. This QVNS circuit has significantly fewer junctions than used in the 2008 work, and this necessitates new modulator bit patterns, but the basic current-pulse biasing scheme and  $f_s = 10\text{ GHz}$  clock are unchanged.

An important distinction for the Gaithersburg QVNS is the use of an older model of semiconductor bit-stream generator with less memory capacity which in practice limits the pattern repetition rate to  $f_1 \sim 1.6\text{ kHz}$ . The more-advanced Boulder system can produce patterns with 4 times lower rates. Another difference lies in the construction of the cryo-probe output cables which in the Boulder system are configured with lower shunt capacitance over the  $\sim 1\text{ m}$  length of the probe. The Gaithersburg QVNS probe is not tuned in this way and hence presents a larger shunt capacitance to the amplifier inputs than is present in the resistance probe. This cable configuration is not significantly different than what was used in our 2008 work. The  $97\ \Omega$  terminations, however, have almost double the resistance of those used in 2008 and this serves to almost double the  $RC$  time constant defining the bandwidth of the source.

The binary patterns of pulses used to generate the pseudo-noise waveforms for each temperature are computed from a delta-sigma algorithm starting from the desired spectral distribution of tones and their specific randomized phase relationships. [4] A single base spectrum with a fixed random phase distribution is used to generate all the necessary QVNS spectra by varying only the amplitudes of the tones to match the spectral density for each  $RT$  product of the resistance probe. The same odd-only harmonic series with a fundamental frequency  $f_1 = 1.589\text{ kHz}$  and  $f_{\max} = 8\text{ MHz}$  as was used in our 2008 work is used here.

## 2.2 Resistance Probe and Measurements

The quartz-sheathed resistance probe is of an identical design to that used in 2008 but has been rebuilt using new silver lead wire and different Pt-8%W alloy resistors. The same quartz insulators are used but these have been inverted so that the hot and cold ends are switched. The use of the same alloy wire in the new resistors (also trimmed to 100  $\Omega$  at 273.15 K) results in  $R(505 \text{ K}) \cong 107 \text{ } \Omega$  and  $R(693 \text{ K}) \cong 113 \text{ } \Omega$  with a temperature coefficient of resistance  $\alpha_R \cong 300 \text{ } \mu\Omega/\Omega$ . A small modification of the probe was made to accommodate purging of the interior with argon gas. This did not have any noticeable effect on the resistance and the probe remained very stable under thermal cycling in the temperature range under investigation.

The resistance of the probe was measured, using a 2-terminal-pair AC resistance bridge operating at 90 Hz excitation, at intervals of  $\sim 2000$  seconds during data acquisition. The reference resistor was a calibrated 100  $\Omega$  non-inductive standard with low AC-DC difference. The bridge had a resolution of 1  $\mu\Omega/\Omega$  and exhibited rms noise on the same level. We assign a combined ( $k=1$ ) measurement uncertainty of 2  $\mu\Omega/\Omega$  for the absolute resistance.

## 2.3 Noise Voltage Correlator Electronics

The two analog channel sections of the noise voltage correlator (NVC) electronics have been replaced with an improved version having approximately 40 dB additional common-mode-rejection ratio.[13] The new design has a similar low-noise preamplifier with an equivalent input noise of 1.4  $\text{nV}\cdot\text{Hz}^{-1/2}$  which is DC coupled to the noise sources, while the old version used in our 2008 work was AC coupled.

Filtering in the new design is accomplished via an 11-pole passive low-pass filter with a 650 kHz 3dB cutoff frequency. This replaces both a 2 MHz 3dB anti-alias active filter stage and the 200 kHz 3dB digital filter which had been used in our previous work in Gaithersburg (and also in the Boulder JNT system prior to  $\sim 2006$ ). These new passive filters are highly stable and define the usable bandwidth of the system. They are utilized in conjunction with

the new amplifier circuits in a buffered configuration as described in the recent paper by Qu, *et. al.* [13] (version 'B' in Figure 1 of [13]).

The Analog-to-Digital Converter (ADC) is the same 14 bit model as described previously [14] that digitizes the amplifier output at 50 MHz, and is followed by Field Programmable Gate Arrays (FPGAs) for additional processing. These FPGAs previously implemented the 200 kHz digital filter, but that function has been disabled in this work so that the only function of the FPGAs now is to accumulate and re-sample the data at 2.083 MHz for optical encoding. The data processing from the optical stream, including Fourier transform and correlation spectra computations, is essentially the same as described in our prior works.[14] The inputs to the NVC are switched between the two sources 'R' and 'Q' every 100 s. The printed-circuit board previously used for switching between sources has been replaced for this work with a new board and new relays, but is of the same design as used in our 2008 work. After publication of our 2008 work, it became clear that the old circuit board was irreversibly damaged by moisture intrusion and that this damage was most likely responsible for the instabilities (primarily drift) encountered in that prior experiment.[3] It should be noted that the design of this switching circuit board is slightly asymmetric with respect to the trace layout for the two inputs (This design is no longer used in the Boulder JNT system having been replaced with a simpler, symmetric, and lower-capacitance version.[1]).

#### 2.4 Comparison Furnace System

The vacuum comparison furnace is the same 3-zone system as described in our prior JNT work.[2] For the present work, however, we use two new Standard Platinum Resistance Thermometers (SPRTs) serial numbers 1528 and 1548. Both of these SPRTs are calibrated at NIST over the ITS-90 subrange between the water triple point and aluminium freezing point [15].

The furnace temperature was continuously measured via the SPRTs, along with other environmental temperatures, at approximately 10 minute cycles. This is accomplished via a second 2-terminal-pair AC resistance bridge also operating at 90 Hz with a calibrated 25  $\Omega$

non-inductive standard reference resistor. The bridge has a resolution of  $25 \mu\Omega$  (0.25 mK) and exhibited rms noise on the same level.

The furnace utilizes two active control zones, an outer ‘guard’ zone, and an inner ‘shell’ zone. A third innermost zone, the ‘core’, passively equilibrates through a weak thermal coupling to the shell and contains the SPRT thermowells and the central thermowell for the noise probe. The furnace core exhibits an rms stability of 0.5 mK at 505 K and typically 2 to 3 mK at 694 K depending on the room temperature control stability.

### **3 Results**

The data described here was obtained over a 3 month period starting in October 2009 and ending in January 2010. Table 1 summarizes the key parameters for each of 4 basic data groups at three separate temperatures. Each data group is a collection of five to seven separate data runs, most of which are between 12 and 16 hours in duration.

#### **3.1 Raw Spectra**

The raw spectra for a given data run consist of the two channels’ power spectra and one cross-correlation spectrum comprising 1,041,667 bins of 0.933 Hz width, for each of the QVNS and resistance probe. The averaged cross-correlation spectrum measures the power of the noise from the resistor or the QVNS only, while the power spectra for each channel of the correlator measure the noise sources plus the uncorrelated noise from the amplifiers. An example of the raw spectra is shown in Figure 2.

#### **3.2 Ratio Spectra for Absolute mode**

In the absolute mode, ratio spectra are formed by re-binning the raw cross-correlated R data as averages of 3200 of the 0.933 Hz bins centred at the location of each QVNS tone starting with the 3<sup>rd</sup> harmonic at 4.768 kHz. The cross-correlated QVNS data is then rebinned in the same way by averaging the central tone with all other bins within a 3200 bin interval out to and including the 375<sup>th</sup> harmonic centered at 596 kHz. These rebinned spectra of 187 bins

each, are then averaged over the entire length of the data run. The two averaged spectra, for each of the R and Q sources, are then used to form a ratio spectrum  $\langle S_R \rangle / \langle S_Q \rangle$  for each run through bin-by-bin division in 3.179 kHz wide bins.

An average ITS-90 temperature  $T_{90}$  is calculated for each run from SPRT data along with an average resistance  $R(T)$  of the R-probe. This data is used to calculate  $S_{R-90} \equiv 4k_B T_{90} R(T)$  and  $X_{90} \equiv S_{R-90} / S_Q$ . By design,  $X_{90}$  is within 0.2 % of unity, but may vary slightly from one run to the next within a data group due to drift in the furnace controls. In order to combine various individual data runs into one grand averaged spectrum for an entire data group we then normalize all the ratio spectra  $S \rightarrow S'$  to be unity when  $T = T_{90}$ . The normalization is accomplished by a simple shift of the origin or  $\langle S'_R \rangle / \langle S'_Q \rangle = \langle S_R \rangle / \langle S_Q \rangle - X_{90} + 1$ . Examples of such normalized absolute ratio spectra for two data groups (Oct 505 and Nov 694) are shown in Figure 3.

The normalized absolute ratio spectra for the four data groups are fit to a 3-parameter even-degree (3PE) model  $a_0 + a_2 f^2 + a_4 f^4$  from 4.8 kHz to 596 kHz. The fitted parameters and their statistical uncertainties are given in Table 2. The statistical uncertainties for the  $a_0$  parameters in the four fitted spectra vary between 22 and 26  $\mu\text{K} \cdot \text{K}^{-1}$ . These are approximately 3 times greater uncertainties than what would be expected for this model over similar integration times and bandwidth.[6] This statistical inflation is caused by distortion in the QVNS waveforms from small non-linear effects in the amplifiers.[13]. Distortion was also present in our 2008 work, however, in the present data the low-frequency distortion products are significantly smaller.

Other correction models which include odd-degree terms may be used for the absolute-mode data as well. Such terms are predicted when insulators in the R and Q input networks exhibit dielectric losses. Given the degree of distortion present in this data and the relatively small magnitude of the odd-degree coefficients, however, it is not possible to distinguish the preferred model from statistical criteria alone. Moreover, when odd-degree terms are allowed, the fitting process will often results in predictions for the  $a_1$  parameter which are unphysical in the magnitude and or the sign. This situation necessitates the adoption of an a priori approach to the estimation of odd-degree terms and this process is discussed in section 4.

### 3.3 Ratio Spectra for Relative Mode

The required ratio spectra for the relative mode are derived from a pair of absolute-mode ratio spectra as indicated by Eq. 5. The relative spectra are computed from bin-by-bin quotients in the four possible combinations of the data groups keeping the 505 K ratio spectra in the denominator. An example of a relative-mode ratio spectrum is shown as the lower trace in Figure 2 for the Nov 694 and Oct 505 data groups. When the same 3PE model is fitted to the relative ratio spectra, the statistical uncertainties in the  $a_0$  parameters are reduced to values between 13 and 16  $\mu\text{K}\cdot\text{K}^{-1}$  compared to  $\sim 34 \mu\text{K}\cdot\text{K}^{-1}$  which would be expected on the basis of combining two uncorrelated absolute ratio spectra. This reduction in uncertainty occurs because the distortion products in the QVNS spectra are mostly stationary and hence correlated from one data group to the next. Table 3a summarized the 3PE fits for the relative spectra.

Another feature of the 3PE fits of the relative-mode ratio spectra is the weak statistical significance of the  $a_4$  term. This is to be expected given that most *LC* coupling terms should be both temperature independent and stationary so that  $\tau_{R,4}(694 \text{ K}) - \tau_{R,4}(505 \text{ K}) \cong 0$ . The model estimates for the relative-mode spectra  $a_4$  coefficient, however, appear to be consistent with the apparent negative drift in time in the  $a_4$  term from the absolute-mode spectra. The statistical significance of this term is therefore slightly higher for the two relative-mode spectra combinations (Nov 694/Jan 505 and Dec 692/Oct 505), which are separated by two months in time rather than only one month.

In our previous work at 693 K we utilized the 3-parameter correction model  $a_0 + a_1 f + a_2 f^2$  out to frequencies of 450 kHz. This 3-parameter model, with both odd and even (3PB) parameters, was necessary due to the existence of a variable dielectric loss in the fibreglass insulation of the switch card used during that experiment. While the dielectric losses are much smaller in the present work, they may not necessarily be negligible. In fact, the relative contribution of the linear term (e.g.  $a_1/a_2$ ) is expected to be greater in the relative-mode spectra than the absolute-mode spectra, so we also calculate 3PB fits for the relative-mode spectra and these are shown in Table 3b. In this case the values for the  $a_1$  coefficients

predicted by the fitting process are within the bounds predicted by an a priori lumped-parameter impedance model (see section 4.1) in three of the four relative ratio spectra.

## 4 Discussion and Uncertainties

In some respects this work is a replication of our earlier 2008 report [3] in that similar methods and equipment have been used. On the other hand, the present work is significantly different in several critical aspects due to improvements made since the completion of the earlier work.

Foremost among these differences is the improved long-term stability of the system in the absolute mode. In our previous work it was necessary to apply a  $6 \mu\text{K}\cdot\text{K}^{-1}\cdot\text{day}^{-1}$  correction in the relative mode to account for an observed systematic drift. Even though an allowance for this correction was made in the uncertainty budget, we still considered this to be a central weakness in that result since, at the time, the origin of the effect was not understood. A drift correction was not necessary in the present work even though the duration of the experiment was approximately four times longer. Replacing the defective circuit board eliminated the most problematic drift and reduced the observed dielectric loss to manageable levels. Small changes were observed, however, in the 505 K absolute ratio spectra during the 3 month time interval, but these were not significant at low frequencies. The details of these and other sources of uncertainty are discussed below.

### 4.1 Correction models

In this work we have utilized both a 3PE model,  $a_0 + a_2f^2 + a_4f^4$ , and a 3PB model,  $a_0 + a_1f + a_2f^2$ , with an upper range limit of 596 kHz. The absence of a linear term in the 3PE model is significant because it improves the statistical uncertainty for the  $a_0$  parameter despite having the same number of model parameters overall. However, there is no clear way to differentiate these two physically plausible models from one another based on statistical considerations alone. Furthermore, other alternative models with more parameters can not necessarily be ruled out based on statistics. This is particularly true in the distortion-limited absolute-mode

spectra and it creates a small degree of ambiguity in the results that we account for with an uncertainty component  $u_{cm}$ .

Fortunately, bounds can be placed on the physically realistic values of any possible  $a_1$  terms through simple lumped-parameter estimations of these terms and knowledge of dielectric losses in the most suspect insulators of the input networks. These are the new switchcard, again made from standard epoxy-fiberboard (FR4), and the sections of quartz insulators used in the R-probe. For the absolute-mode spectra we estimate the sign and magnitude of any linear frequency term via

$$a_{1-Est} \approx 2\pi \{ (2R_Q - [2 - T_{FR4}/T]R(T)) C_{FR4} \tan \delta_{FR4} - [2 - T_{qz}/T]R(T) C_{qz} \tan \delta_{qz} \} \quad (7)$$

where:  $R_Q$  is the single-end series termination resistance of the QVNS probe;  $R(T)$  is the differential resistance of the R-probe;  $C_{FR4}$  is the effective shunt capacitance for the FR4 dielectric in the switch card traces (assumed to be equal for R and Q inputs);  $\tan \delta_{FR4}$  is the associated loss tangent for the FR4 dielectric;  $T_{FR4}$  is the switch-card temperature; and  $C_{qz}$ ,  $\tan \delta_{qz}$  and  $T_{qz}$  are the effective shunt capacitance, loss tangent, and temperature, respectively, for the hot sections of the quartz insulators in the R-probe. Equation 7 is a superposition of the noise from  $R$  attenuated by the  $RC$ -filter and the noise the capacitances similarly attenuated. Only those capacitances in the R-network contribute correlated noise since the two halves of the Q-network are decoupled by the QVNS source. Given realistic values for all of the physical parameters, we estimate  $a_{1-Est}(505) \approx +6(4) \times 10^{-8} \text{ kHz}^{-1}$  and  $a_{1-Est}(694) \approx -5.4(7.7) \times 10^{-8} \text{ kHz}^{-1}$  for the absolute-mode spectra. These a priori predictions are small in magnitude but highly uncertain. Attempts to fit the absolute spectra to a model with a linear coefficient as a free parameter results in fitted values for  $a_1$  outside of these bounds (i.e. unphysical) and of marginal statistical significance.

As an alternative to fitting the  $a_1$  parameter, the effects of small dielectric losses on the measured absolute noise temperatures can be accessed by including a liner term with fixed  $a_1$  and refitting the data to the 4<sup>th</sup> degree polynomial ( $a_3=0$ ). We have used a Monte-Carlo simulation to sample values of  $a_1$  from a uniform distribution within the range predicted by Eqn. 7 for assessing the correlation between fitted values of  $a_0$  and assumed values of  $a_1$  for

the absolute-mode data. The results yield a weak, linear-negative correlation between changes  $\Delta a_0$  as a function of changes  $\Delta a_1$  from the assumed distribution of  $a_1$  and these are given in Table 4. When these correlations are applied as corrections to the 3PE model results, the  $a_0$  values for the 505 K data are shifted down by  $\sim 4 \mu\text{K}\cdot\text{K}^{-1}$  and the 694 K data are shifted up by approximately the same amount. The uncertainties in making these corrections are  $\sim 3 \mu\text{K}\cdot\text{K}^{-1}$  and  $5.6 \mu\text{K}\cdot\text{K}^{-1}$  respectively.

Another implicit assumption being made in the approximations leading to Eqn. 7 is that the loss tangents are frequency independent. This is not always the case, but the degree of frequency dependence observed in these insulators is normally very weak over the frequencies of interest here. Given the uncertain nature of these corrections, together with the lack of quantitative estimates on the size of  $a_3$  (which we ignore in this work) and the related model ambiguities, we assign an overall correction model uncertainty of  $u_{\text{cm}}=20 \mu\text{K}\cdot\text{K}^{-1}$  for the absolute-mode data.

The estimate for the  $a_1$  parameter for the relative-mode spectra is given by the difference of the absolute-mode estimated coefficients  $a_{1\text{-Est}}(694)$  and  $a_{1\text{-Est}}(505)$  or  $a_{1\text{-Est}}(694/505) \approx -1.1(0.4)\times 10^{-7} \text{ kHz}^{-1}$ . Three of the four 3PB fits shown in Table 3b yield fitted values of  $a_1$  which are within the bounds of this estimate (i.e.  $a_{1\text{-Est}} \leq a_1 \pm u(a_1) \leq 0$ ). In light of these observations, we view the 3PB fits to be the more physically correct model appropriate for the relative-mode ratio spectra of this work. When averaged over all spectral combinations, the difference between the  $a_0$  parameter as derived by the 3PE and 3PB fits is only  $\sim 10 \mu\text{K}\cdot\text{K}^{-1}$ , which is within the statistical uncertainties of either model's estimates. We assign an additional type B uncertainty  $u_{\text{cm}}=10 \mu\text{K}\cdot\text{K}^{-1}$  to account for the remaining small degree of ambiguity for the relative spectra correction model.

#### 4.2 Non-linearity and Distortion

The presence of distortion is evident in the absolute-mode spectra and, as already discussed in section 3, this distortion is the dominant source of dispersion limiting the statistical precision for the correction model. The correlation coefficients for pairs of residuals of the 3PE fits to the absolute-mode spectra vary between approximately 0.78 and 0.88 (see Table 5), which is

consistent with the observation that the majority of the distortion remained stationary throughout the experiment.

Some distortion, however, was of a variable nature. The degree to which the variable distortion influences the correction models is most readily estimated by comparing the results for the 3PE fits of the Oct505 and Jan505 absolute spectra. Since the  $a_0$  parameters differ by only  $11 \mu\text{K}\cdot\text{K}^{-1}$  with  $26 \mu\text{K}\cdot\text{K}^{-1}$  statistics, we conclude that any bias effect from variable distortion is unresolvable. Hence, we allow a small uncertainty component of  $11 \mu\text{K}\cdot\text{K}^{-1}$  in the absolute spectra and  $3.7 \mu\text{K}\cdot\text{K}^{-1}$  in the relative spectra for the possible bias effects (i.e. non-statistical) due to distortion, both variable and stationary.

#### 4.3 EMI

The presence of narrow band EMI harmonics, starting at  $\sim 26$  kHz, is evident in the QVNS raw spectra as shown in Figure 2. This EMI remained relatively stationary during the entire duration of the experiment. Similar EMI could also be present in the R spectra, but if comparable in amplitude it would remain unresolved compared to the much higher continuous correlated noise spectral density of the R probe. Even if this EMI was only present in the QVNS spectra, the net effect on the ratio spectra would still be negligible since it is limited to only a few 0.963 Hz frequency bins and more than  $-40$  dBc in relative magnitude for the four to five resolvable harmonics.

As was indicated in section 3.2, the re-binning method employed in this work averages all the data over the 3200 of the 0.983 Hz bins surrounding any given QVNS tone. This has been referred to as a ‘Bin’ analysis in prior works. This is in distinction to the ‘Peak’-analysis method used for computing results in our prior 2008 work which ignored the content of all other bins that did not contain the QVNS tone. In this work, we compared spectra from individual data runs using the Bin- and Peak-analysis methods, and in all cases the results differed by less than the statistical precision of either result and were often  $< \sim 10 \mu\text{K}\cdot\text{K}^{-1}$ . This difference is a measure of both the effects of EMI in the QVNS spectra and the presence of aliased tones.

Low-level EMI that could be present in the R-spectra alone is not readily detectable. If such EMI contamination did exist and was stationary, it would affect the results of the absolute-mode spectra but cancel in the relative-mode spectra. Non-stationary EMI would be expected to affect the relative-mode results slightly more than in the absolute-mode results. In this work the results from the two modes at 693 K agree to well within the statistical bounds. Under the assumption that equal but uncorrelated amounts of stationary and non-stationary EMI are corrupting all the absolute spectra resulting in errors of  $\sim 10 \mu\text{K}\cdot\text{K}^{-1}$  each, the net effect on both the absolute spectra and the relative spectra would be a probable error of  $14 \mu\text{K}\cdot\text{K}^{-1}$ . We therefore assign a type B EMI uncertainty component of  $u_{\text{EMI}}=14 \mu\text{K}\cdot\text{K}^{-1}$  for both the absolute mode relative mode results.

#### 4.4 Stability

The system is designed to account for most forms of instability or drift. Drift in the amplifier gains is automatically cancelled by alternate switching of the inputs. Drift in the input network impedances is accounted for by grouping the data into contiguous time intervals which were never greater than 24 days and in most cases less than 2 weeks in length. Other longer-term drift can occur, such as the trend that is observed in the  $a_4$  coefficient in the absolute-mode spectra, but this is complicated by other concurrent changes that may occur in both the EMI and distortion products. This is most readily observed by forming a relative spectrum from the Oct505 and Jan505 spectra spanning a 3 month time difference. This spectrum is shown in Figure 4 and exhibits a structural pattern that can not be fitted by either the 3PE or the 3PB correction models. The spectrum exhibits a more complex pattern with either a higher-degree even characteristic or 4<sup>th</sup>-degree with significant odd-degree terms. We interpret this as a variable distortion pattern superimposed with slowly variable input-network time constants. The variable distortion is generated by changes in non-linear processes of the amplification chain, either from environmental changes such as ambient temperature and humidity or possibly also from out-of-band EMI.

When similar relative-mode spectra are formed from absolute-mode spectra taken at the same temperature but with shorter time differences, the resulting relative-mode spectra appear

random, with no apparent structure like that of Figure 4. Furthermore, the excellent agreement between the two relative-mode ratio spectra, Nov 694/Oct 505 and Dec692/Jan 505, could not occur under a secular systematic drift since their relative time differences are of the opposite sign. We conclude that, whatever the origin of the long-term drift exhibited in Figure 4, its influence on the  $a_0$  parameter of the correction models is small, particularly for the relative ratio spectra which are formed from data separated by less than 1 month (i.e. Nov 694/Oct 505 and Dec692/Jan 505). We therefore do not include any uncertainty component for instability.

#### 4.5 QVNS reference spectra

The quantized nature of the voltages produced by the QVNS and its wide bandwidth ensure that the uncertainties arising from the QVNS are small. However, there is still potential for errors, and the most significant error contribution comes from undesired nonquantized signals associated with the current sources biasing the QVNS, such as input-output coupling and bias currents driving inductance in the QVNS circuit. These errors, which fortunately have been undetectable thus far, are most significant at higher frequencies, so they would likely be removed through the fitting analysis.

The absolute uncertainty of the local master clock also contributes to the QVNS output uncertainty. The Gaithersburg JNT system uses a 10 MHz oven-stabilized crystal oscillator timebase for the reference clock which synchronizes both the ADCs and the 10 GHz clock for the bit stream generator. The master clock uncertainty is  $\sim 0.1 \mu\text{Hz}\cdot\text{Hz}^{-1}$  which has been verified by comparison with a rubidium frequency standard. The estimated timebase drift is  $0.01 \mu\text{Hz}\cdot\text{Hz}^{-1}\cdot\text{year}^{-1}$  or  $0.0025 \mu\text{Hz}\cdot\text{Hz}^{-1}$  uncertainty in the relative mode over the 90 day duration of the experiment.

#### 4.6 Resistance Measurements

As already discussed in section 2.2 above, we assign a combined measurement uncertainty of  $2 \mu\Omega/\Omega$  for the absolute resistance. For the relative-mode spectra, we assign an uncertainty of  $1 \mu\Omega/\Omega$  for the resistance ratio  $R(694 \text{ K})/R(505 \text{ K})$ .

#### 4.7 Spectral Aberrations

Several errors in the fidelity of absolute-mode noise ratio spectra can occur due to limitations in comparing continuous versus discrete spectra. Some of these have been treated by White and Benz [8] and the effects are most noticeable beyond 500 kHz for the type of low-pass filter employed in this work. These effects are currently unresolvable, however, due to the much higher distortion levels present in the ratio spectra of this work.

Other types of spectral aberrations can occur due to digital sampling errors, or aliasing. It has been shown by Qu, *et. al.* [13] that the passive filters used here have a finite power stop band of  $-80$  dBc, or a voltage stop band of  $-40$  dBc. This filter limitation allows aliased spectral content to contaminate the true spectra by relative amounts as large as  $100 \mu\text{V}\cdot\text{V}^{-1}$ . Since in this work we do not use a second low-pass filter to further suppress aliasing (as has been done for the Boulder JNT system) the present results are susceptible to this type of error. We assume, however, that the only aliasing errors that would matter in the absolute-mode spectral ratio would be those which are different for the R and Q spectra and would be evident through comparison of Bin and Peak-averaged spectra as described in section 4.3. A  $10 \mu\text{K}\cdot\text{K}^{-1}$  uncertainty estimate for the absolute mode accounts for these effects. We further assume that any such aliasing effects would cancel in the relative-mode ratio spectra.

#### 4.8 ITS-90

The uncertainties associated with ITS-90 temperatures are shown in Table 6. These include contributions from measurement statistics, calibration, stability, temperature non-uniformity, and resistance ratios. The two SPRTs, s/ns 1528 and 1548, were in good agreement ( $\Delta T_{90} \leq 1$  mK) during the 3 month interval of the experiment. The maximum observed change in these two SPRTs WTP value was 0.4 mK during a 6-month period including the 3 months of the experiment.

#### 4.9 Total Combined Uncertainty

The uncertainty budget for the noise measurements is shown on Table 7 along with a summary of the ITS-90 uncertainties and the total combined uncertainties for  $\varepsilon_{\text{am}}(505 \text{ K})$  and

$\varepsilon_{\text{am}}(693 \text{ K})$  in the absolute mode and  $\varepsilon_{\text{rm}}(693 \text{ K})$  in the relative mode. An additional  $1.7 \mu\text{K}\cdot\text{K}^{-1}$  uncertainty contribution from  $k_{\text{B}}$  is required in the absolute mode, while the uncertainty in  $K_{\text{J}}$  is only  $0.05 \mu\text{K}\cdot\text{K}^{-1}$ . These contributions do not enter into the relative mode uncertainty.

#### 4.10 Determination of Noise Temperatures

The results for the absolute spectra are summarized in Table 8 in terms of  $\varepsilon \equiv a_0 - 1 = T/T_{90} - 1$  (i.e., relative to ITS-90) expressed in  $\mu\text{K}\cdot\text{K}^{-1}$  and  $T - T_{90}$  expressed in mK together with their *combined* standard uncertainties. These results are derived from the 3PE model correction and the a priori correction for  $a_1$  in Table 4. The average (Oct505 and Jan505) absolute noise temperature  $\varepsilon_{\text{Sn}} = +13 \mu\text{K}\cdot\text{K}^{-1}$  agrees well, within our standard combined uncertainty of  $39 \mu\text{K}\cdot\text{K}^{-1}$ , with the much less uncertain result from Strouse *et. al.* [16]

The values of  $a_0 - 1$  from the relative-mode spectra represent differences in the relative temperature difference or  $\varepsilon_{\text{Zn}} - \varepsilon_{\text{Sn}}$ . If the ITS-90 value for the Sn freezing point (505.078 K) were assumed to be thermodynamically correct, then  $\varepsilon_{\text{Sn}} = 0$  and the relative noise temperature for the Zn freezing point would be equivalent to  $a_0 - 1$  (i.e. derived from Table 3b). In contrast, we make a correction to the ITS-90 using the best available thermodynamic determination of that temperature as derived via Acoustic Gas Thermometry (AGT) from Strouse, *et. al.* [16] of  $\varepsilon_{\text{Sn-AGT}} = +21.2 (5.9) \mu\text{K}\cdot\text{K}^{-1}$ . This same procedure was used in our 2008 Zn FP determination. The results for the as-corrected relative-mode spectra are summarized in Table 9 together with combined standard uncertainties using the two statistically-independent combinations of data groups: Nov 694/Oct 505 and Dec692/Jan 505. The absolute and relative mode results at 692 and 694 K are self-consistent. When the two data group combinations for 692 K and 694 K are combined, the result is  $\varepsilon_{\text{Zn}} = 5.7 \pm 25 \mu\text{K}\cdot\text{K}^{-1}$  or  $T - T_{90} = +4 \pm 18 \text{ mK}$ .

## 5 Conclusions

We have replicated a series of noise temperature measurements which re-determine the noise temperature for zinc freezing point relative that of the Sn freezing point. Our new relative mode value for the Zn freezing point is  $\varepsilon_{Zn}(693\text{ K}) = +6 \pm 25 \mu\text{K}\cdot\text{K}^{-1}$  or  $T-T_{90} = +4 \pm 18\text{ mK}$ . In addition we report, for the first time in this range, absolute noise temperature results of  $T-T_{90} = +6.7 \pm 20\text{ mK}$  for the Sn FP and  $T-T_{90} = -2.5 \pm 27\text{ mK}$  for the Zn FP. Comparisons of these results to our past JNT results and with other recent literature values from Infrared Filter Radiometry are shown in Table 10. The results from this and our 2008 Quantized voltage-based JNT determinations are in good agreement with the filter radiometry.

### **Acknowledgments**

We gratefully acknowledge the important work of Jifeng Qu while serving as a guest researcher at NIST Boulder, enabling technical advances which benefited this work in Gaithersburg. We also gratefully acknowledge Charlie Burroughs for chip packaging and Sae Woo Nam and John Martinis for their important contributions in the earliest development stages of NIST JNT programs. Special thanks go to Greg Strouse for SPRT calibrations. We received helpful comments from XXXXXXXXXXXX and YYYYYYYYYY.

## References

- [1] S. Benz, J. Qu, H. Rogalla, D. White, P. Dresselhaus, W. Tew, and S. Nam, "Improvements in the NIST Johnson Noise Thermometry System," *IEEE Trans. Instrum. Meas.*, vol. 58, Apr. 2009, pp. 884-890.
- [2] W. Tew, J. Labenski, S. Nam, S. Benz, P. Dresselhaus, and C. Burroughs, "Johnson noise thermometry near the zinc freezing point using resistance-based scaling," *Intern. J. Thermophys.*, vol. 28, Apr. 2007, pp. 629-645.
- [3] J. Labenski, W. Tew, S. Benz, S. Nam, and P. Dresselhaus, "A determination of the ratio of the zinc freezing point to the tin freezing point by noise thermometry," *Intern. J. Thermophys.*, vol. 29, Feb. 2008, pp. 1-17.
- [4] S. Benz, J. Martinis, P. Dresselhaus, and S. Nam, "An AC Josephson source for Johnson noise thermometry," *IEEE Trans. Instrum. Meas.*, vol. 52, Apr. 2003, pp. 545-549.
- [5] S. Benz, D. White, J. Qu, H. Rogalla, and W. Tew, "Electronic measurement of the Boltzmann constant with a quantum-voltage-calibrated Johnson noise thermometer," *Comp. Rend. Physique*, vol. 10, Nov. 2009, pp. 849-858.
- [6] D.R. White, S.P. Benz, J.R. Labenski, S.W. Nam, J.F. Qu, H. Rogalla, and W.L. Tew, "Measurement time and statistics for a noise thermometer with a synthetic-noise reference," *Metrologia*, vol. 45, 2008, pp. 395-405.
- [7] S. Benz, J. Martinis, S. Nam, W. Tew, and D. White, "A new approach to Johnson Noise Thermometry using a Josephson quantized voltage source for calibration," *TEMPMEKO 2001: 8TH Inter. Symp. Temp. Thermal*, 2002, pp. 37-44.
- [8] D.R. White and S.P. Benz, "Constraints on a synthetic-noise source for Johnson noise thermometry," *Metrologia*, vol. 45, 2008, pp. 93-101.
- [9] J. Labenski, W. Tew, S. Nam, S. Benz, P. Dresselhaus, and C. Burroughs, "Resistance-based scaling of noise temperatures from 1 kHz to 1 MHz," *IEEE Trans. Instrum. Meas.*, vol. 56, Apr. 2007, pp. 481-485.
- [10] D.R. White and E. Zimmermann, "Preamplifier limitations on the accuracy of Johnson noise thermometers," *Metrologia*, vol. 37, 2000, pp. 11-23.
- [11] S.W. Nam, S.P. Benz, J.M. Martinis, P. Dresselhaus, W.L. Tew, and D.R. White, "A Ratiometric Method for Johnson Noise Thermometry Using a Quantized Voltage Noise Source," *TEMPERATURE: Its Measurement and Control in Science and Industry; Volume VII; Eighth Temperature Symposium*, D.C. Ripple, Ed., Chicago, Illinois (USA): AIP, 2003, pp. 37-42.
- [12] S. Benz and C. Hamilton, "A pulse-driven programmable Josephson voltage standard," *App. Phys. Lett.*, vol. 68, May. 1996, pp. 3171-3173.
- [13] J. Qu, S.P. Benz, H. Rogalla, and D.R. White, "Reduced non-linearities and improved temperature measurements for the NIST Johnson noise thermometer," *Metrologia*, vol. 46, 2009, pp. 512-524.
- [14] S. Nam, S. Benz, P. Dresselhaus, W. Tew, D. White, and J. Martinis, "Johnson noise thermometry measurements using a quantized voltage noise source for calibration," *IEEE Trans. Instrum. Meas.*, vol. 52, Apr. 2003, pp. 550-554.
- [15] B.W. Mangum and G. Furukawa, *Guidelines for Realizing the International Temperature Scale of 1990 (ITS-90)*, Gaithersburg, MD: U.S. Dept. of Commerce, National Institute of Standards and Technology, 1990.
- [16] G.F. Strouse, "Progress in Primary Acoustic Thermometry at NIST: 273 K to 505 K," *AIP Conference Proceedings*, Chicago, Illinois (USA): 2003, pp. 31-36.
- [17] D.R. Taubert, J. Hartmann, J. Hollandt, and J. Fischer, "Investigation of the Accuracy of the ITS-90 with Reference to Thermodynamic Temperature in the Range from 400 [degree]C up to 600 [degree]C," *TEMPERATURE: Its Measurement and Control in*

*Science and Industry; Volume VII; Eighth Temperature Symposium*, D.C. Ripple, Ed., Chicago, Illinois (USA): AIP, 2003, pp. 7-12.

- [18] N. Noulkow, R. Taubert, P. Meindl, and J. Hollandt, "Infrared Filter Radiometers for Thermodynamic Temperature Determination below 660 °C," *International Journal of Thermophysics*, vol. 30, Feb. 2009, pp. 131-143.

**Table 1.** Data Summary

Data Group ID	Dates <sup>a</sup>	Total time duration (Hours)	Average Temperature (K)
Oct 505	22-Oct to 30 Oct 09	82	505.27
Nov 694	16-Nov to 20-Nov	62	693.94
Dec 692	30-Nov & 16-Dec to 23 Dec	61	692.49
Jan 505	5-Jan to 18-Jan-2010	87	505.30

<sup>a</sup> The Dates listed are the range over which data was obtained, but do not necessarily correspond to continuous time intervals.

**Table 2.** 3PE Fitting parameters and statistical uncertainties for the absolute spectra

Data Group ID	$a_0$	$a_2$ (kHz <sup>-2</sup> )	$a_4$ (kHz <sup>-4</sup> )
Oct 505	1.000023 (26)	3.16 (.04) e-08	-2.8 (1.3) e-15
Nov 694	0.999991 (22)	2.72 (.04) e-08	-3.6 (1.2) e-15
Dec 692	0.999994 (23)	2.74 (.04) e-08	-4.0 (1.2) e-15
Jan 505	1.000012 (26)	3.26 (.05) e-08	-4.4 (1.4) e-15

**Table 3a.** 3PE correction model parameters for the relative spectra

Data Group Combination	$a_0$	$a_2$ (kHz <sup>-2</sup> )	$a_4$ (kHz <sup>-4</sup> )
Nov 694/Oct 505	0.999968 (13)	-4.37 (0.23) e-09	-6.4 (7.1) e-16
Nov 694/Jan 505	0.999979 (13)	-5.42 (0.22) e-09	9.9 (6.7) e-16
Dec 692/Oct 505	0.999971 (16)	-4.18 (0.28) e-09	-1.08 (0.86) e-15
Dec 692/Jan 505	0.999982 (13)	-5.24 (0.23) e-09	5.5 (7.0) e-16

**Table 3b.** 3PB correction model parameters for the relative spectra

Data Group Combination	$a_0$	$a_1$ (kHz <sup>-1</sup> )	$a_2$ (kHz <sup>-2</sup> )
Nov 694/Oct 505	0.999984 (22)	-7.64 (0.17) e-08	-4.44 (0.27) e-09
Nov 694/Jan 505	0.999966 (20)	1.63 (0.16) e-08	-5.14 (0.25) e-09
Dec 692/Oct 505	1.000003 (26)	-1.7 (2.0) e-07	-4.25 (0.32) e-09
Dec 692/Jan 505	0.999985 (21)	-8.2 (16) e-08	-4.94 (0.26) e-09

**Table 4.** Summary of a priori dielectric loss corrections to the 3PE model for absolute-mode data.

	Oct 505	Nov 694	Dec 692	Jan 505
$a_{1\text{-Est}}$ kHz <sup>-1</sup>	+6(4)E-8	-5.4(7.7)E-8	-5.4(7.7)E-8	+6(4)E-8
$\Delta a_0/\Delta a_1$ kHz	-6.9E+07	-7.3E+07	-7.1E+07	-7.1E+07
$\Delta a_0$ ( $\mu\text{K}\cdot\text{K}^{-1}$ )	-4.2	3.9	3.8	-4.3
corrected [ $a_0 - 1$ ] ( $\mu\text{K}\cdot\text{K}^{-1}$ )	18.8	-5.1	-2.2	7.7

**Table 5.** Correlation coefficients for the 3PE residuals of absolute spectra pairs.

Data Group Pair	Nov 694, Oct 505	Nov 694, Jan 505	Dec 692, Jan 505	Dec 692, Oct 505	Nov 694, Dec 692	Oct 505, Jan 505
$C_{1,2}$	0.852	0.879	0.867	0.781	0.838	0.871

**Table 6.**ITS-90 Uncertainties

	505 K mK	692 K-694 K mK
Statistics	0.5	3
non-uniformity	1	3
R-probe immersion	1	2
Resistance Ratio	0.25	0.25
Calibration	0.1	0.25
Stability	0.5	3
RSS	1.6	5.6

**Table 7.** Noise measurement (type A and type B) and Combined Uncertainties for the Absolute Mode and Relative Mode determinations.

	Absolute $\mu\text{K}\cdot\text{K}^{-1}$	Relative $\mu\text{K}\cdot\text{K}^{-1}$	Absolute 693 K mK	Absolute 505 K mK	Relative 693 K mK
Statistics (A)	26	21	18.0	13.1	14.6
Correction Model (B)	25	10.0	13.9	10.1	6.9
EMI (B)	14	14	9.7	7.1	9.7
QVNS (B)	0.1	<0.1	0.07	0.05	<0.07
Resistance (B)	2	1.0	1.4	1.0	0.7
Non-Lin. & Distortion (B)	11	3.7	7.6	5.6	2.5
Spec. Aberrations (B)	10		7	5	
Fund. Constants (B)	1.7		1.2	0.9	
RSS B	29	18	20	15	12
RSS A+B	39	27	27	20	19
ITS90					
505 K	3.2	–	–	1.6	–
693 K	8.1	9	5.6	–	6.0
AGT Correction to 505 K	–	5.9	–	–	4.1
Combined Total Uncertainty					
505 K	39	–	–	20	–
693 K	40	29	27	–	20

**Table 8.** Summary of results and combined standard uncertainties of absolute noise temperatures from the absolute ratio spectra of the four data groups based on 3PE model +  $a_1$  a priori corrections with respect to ITS-90.

Data Group	$(T-T_{90})/T_{90}$ $\mu\text{K}\cdot\text{K}^{-1}$	$T-T_{90}$ (mK)
Oct 505	19 (39)	9.5 (20)
Nov 694	-5 (40)	-3.5 (27)
Dec 692	-2 (40)	-1.4 (27)
Jan 505	8 (39)	3.4 (20)

**Table 9.** Summary of results with respect to ITS-90 and combined standard uncertainties from the relative ratio spectra as corrected to AGT results at 505 K and the 3PB model.

Data Group Combination	$T_{90}$ K	$(T-T_{90})/T_{90}$ $\mu\text{K}\cdot\text{K}^{-1}$	$T-T_{90}$ (mK)
Nov 694 / Oct 505	693.94	5 (29)	3.6 (20)
Dec 692 / Jan 505	692.49	6 (29)	4.3 (20)

**Table 10.** Comparison of recent literature values for  $T-T_{90}$  near the Zn FP, in mK.

Citation, Year	Taubert, <i>et. al.</i> 2003 [17]	Noulkow, <i>et.al.</i> 2007[18]	Noulkow, <i>et.al.</i> 2007[18]	Tew, <i>et. al.</i> 2007[2]	Labenski, <i>et. al.</i> 2008[3]	This Work 2010
Method	IRFR <sup>a</sup> 1 $\mu\text{m}$	IRFR 1.3 $\mu\text{m}$	IRFR 1.55 $\mu\text{m}$	RR-JNT <sup>b</sup>	RQ-JNT <sup>c</sup>	RQ-JNT
$T-T_{90}$	$41 \pm 45$	$28 \pm 29$	$10 \pm 34$	$-7 \pm 31^{\text{d}}$	$+7 \pm 30$	$+4 \pm 18$

a. Infrared Filter Radiometry

b. Relative Resistance-based Johnson Noise Thermometry

c. Relative Quantized voltage-based Johnson Noise Thermometry

d. Adjusted by  $+10 \mu\text{K}\cdot\text{K}^{-1}$  from as-published value due to a statistical offset.[6]

## Figure Captions

**Fig. 1** Functional diagram of the JNT measurement system in the NIST Gaithersburg facility. NVC, Noise Voltage Correlator electronics; S, switching network; Gx,Gy, Analog Gain blocks and digitizers; Code Gen.: Bit stream generator with 10 GHz clock. (See text)

**Fig. 2** Raw QVNS and R-probe spectra with  $\sim 1$  Hz wide bins.

**Fig. 3** The Absolute ratio spectra for the Nov 694 and Oct 505 data groups and the relative ratio spectrum derived by their combination.

**Fig. 4** The ratio of the Jan 505 K spectrum to the Oct 505 K spectrum showing changes in the input network time constants, EMI, and distortion products that took place over the 3 month time interval of the experiment.

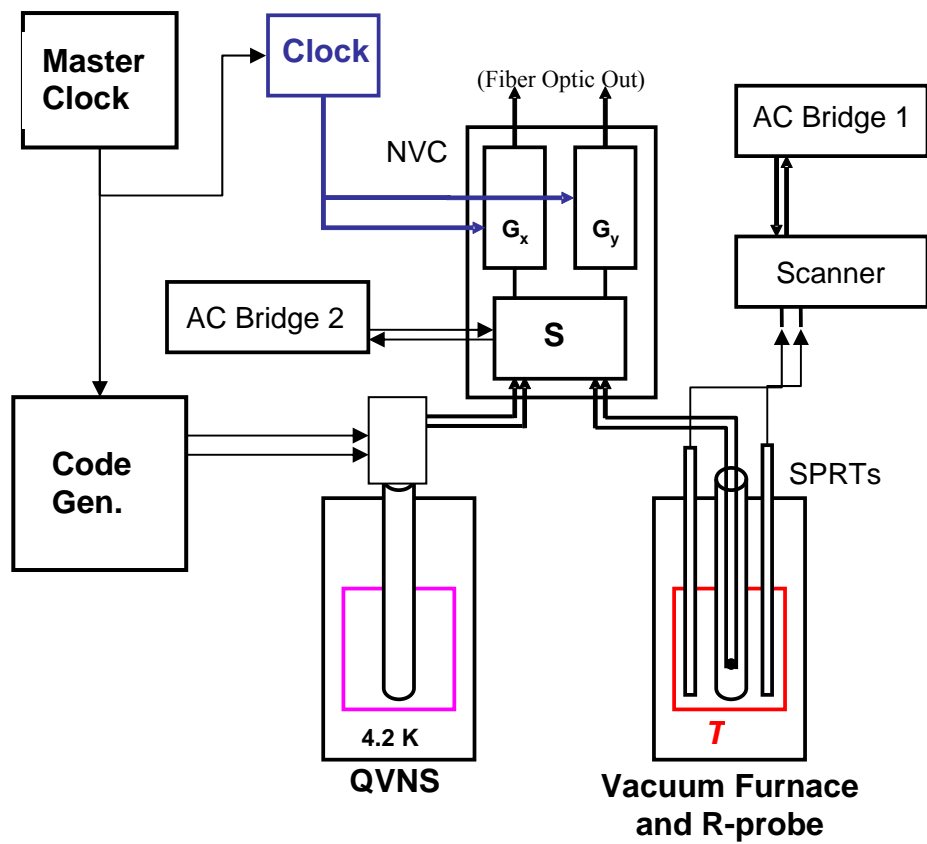
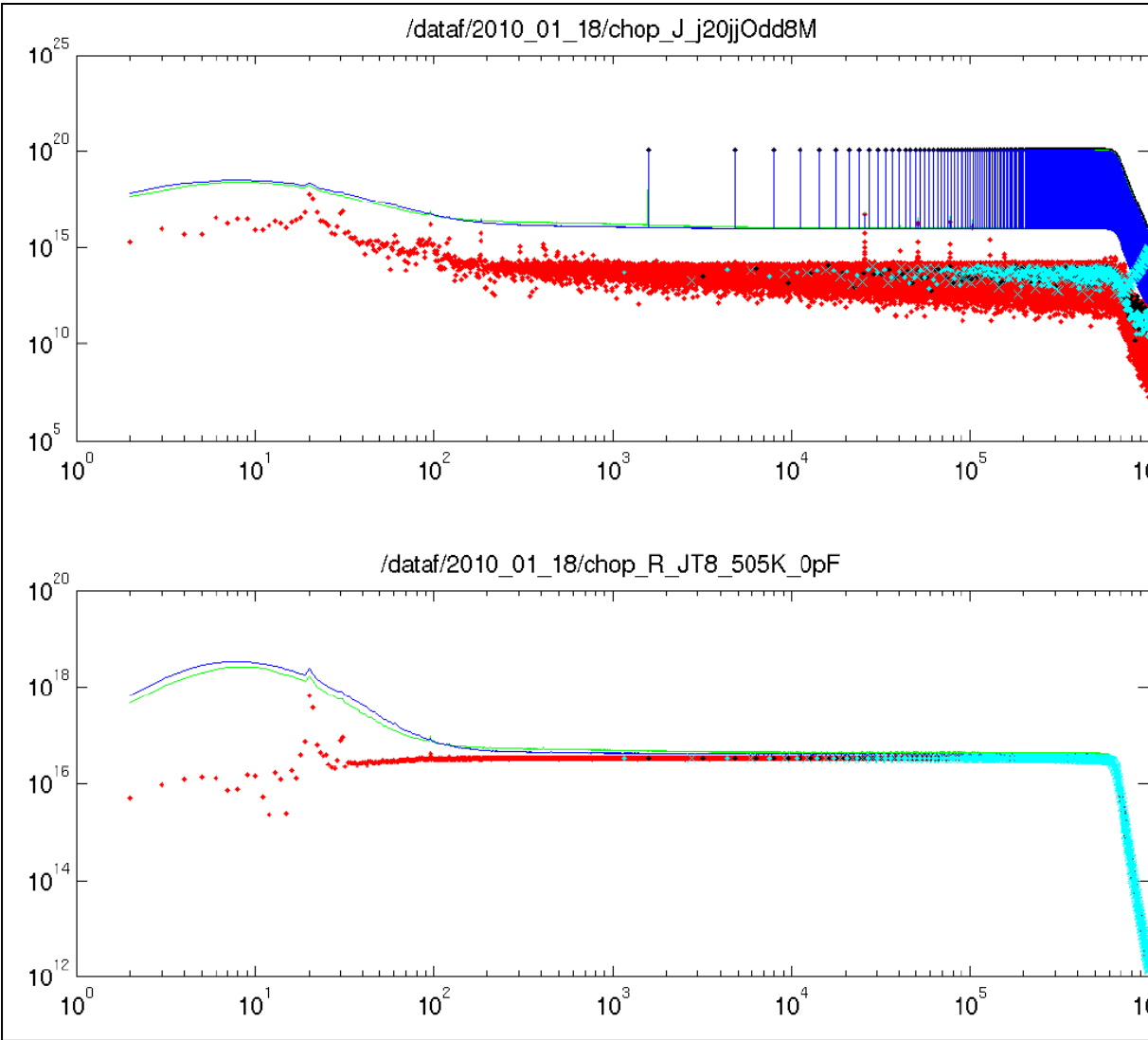


Figure 1



$f, \text{ Hz}$

Figure 2 (To Be Replaced with improved version)

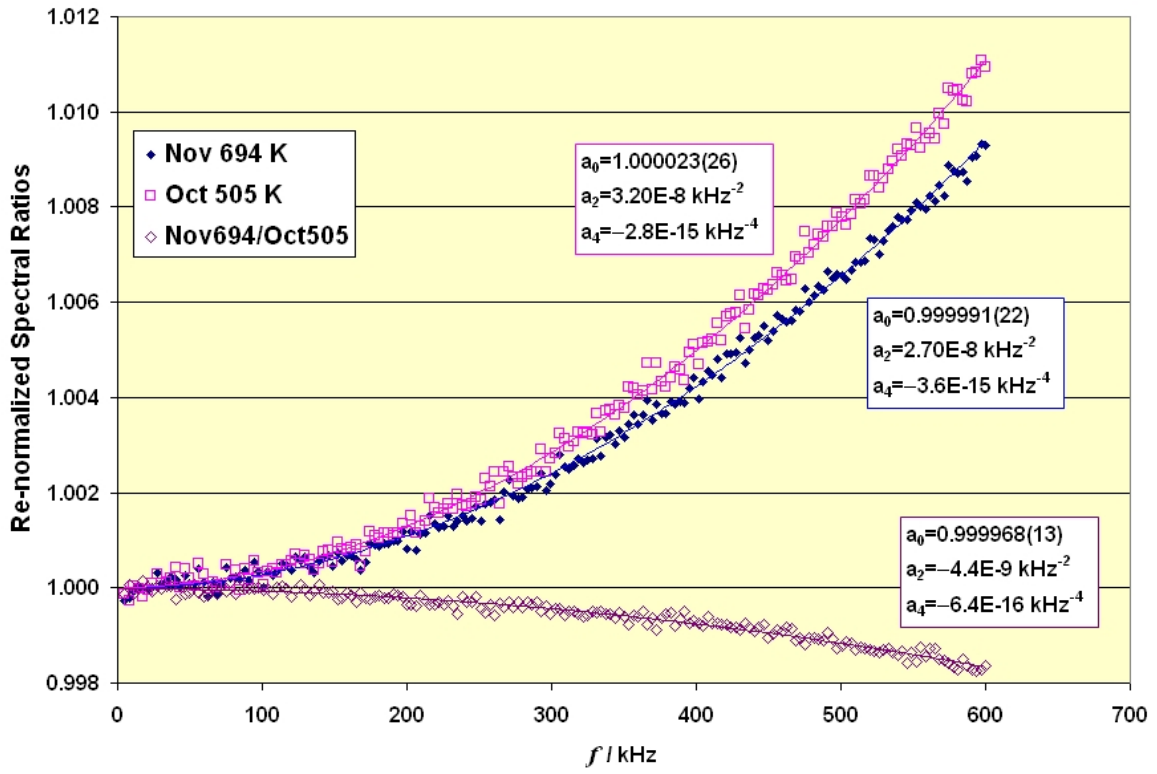


Figure 3.

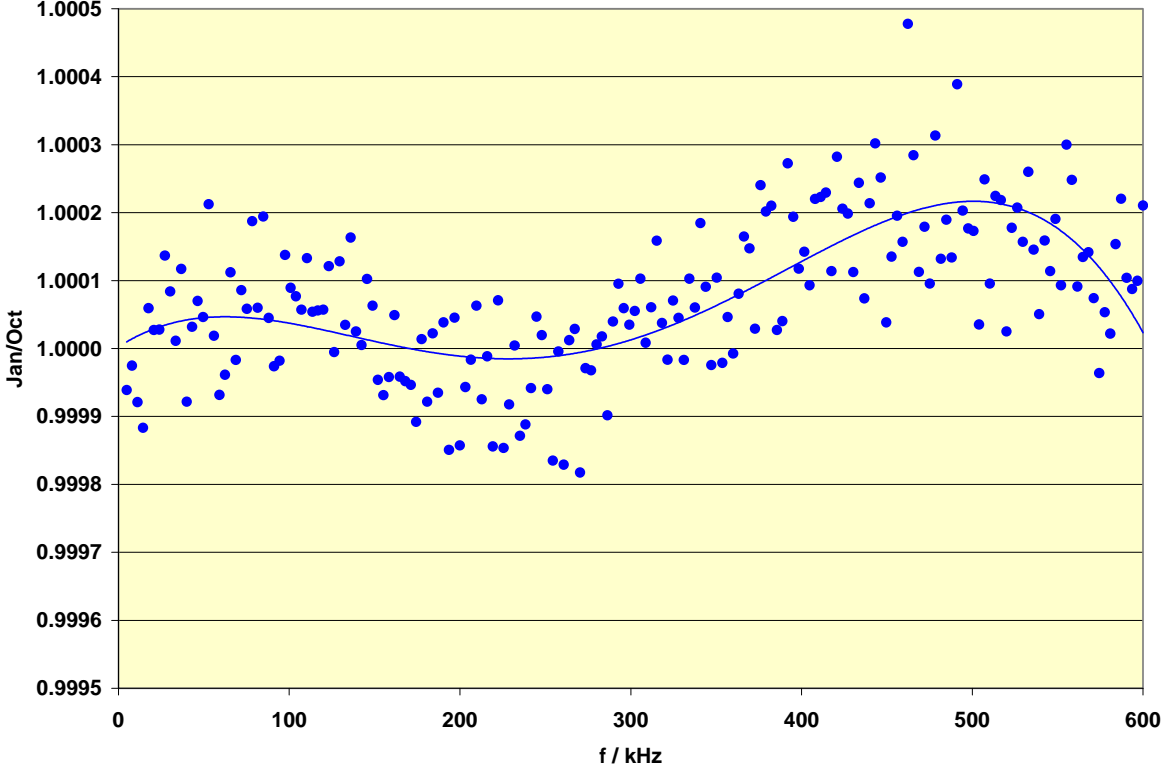


Figure 4.